



Geophysical Research Letters

Supporting Information for

Earthquake damage patterns resolve complex rupture processes

Yann Klinger¹, Kurama Okubo^{1,2}, Amaury Vallage^{1†}, Johann Champenois^{1,3}, Arthur Delorme¹, Esteban Rougier⁴, Zhou Lei⁴, Earl E. Knight⁴, Antonio Munjiza⁵, Claudio Satriano¹, Stephane Baize³, Robert Langridge⁶ and Harsha S. Bhat²

¹Institut de Physique du Globe de Paris, Sorbonne Paris Cité, Université Paris Diderot, CNRS, Paris, France.

²Laboratoire de Géologie, École Normale Supérieure/CNRS UMR8538, PSL Research University, Paris 75005, France

³Seismic Hazard Division, Institut de Radioprotection et de Sécurité Nucléaire, Fontenay-aux-Roses, France

⁴EES-17 – Earth and Environmental Sciences Division, Los Alamos National Laboratory, NM, USA

⁵FGAG– University of Split, 21000 Split, Croatia.

⁶GNS Science, P.O. Box 30-368, Lower Hutt, 5040, New Zealand.

† now at CEA, DAM, Arpajon_91297, France

Contents of this file

Text S1 to S3
Figures S1 to S7
Tables S1

Additional Supporting Information (Files uploaded separately)

Captions for Movies S1 to S2

Introduction

Supplementary information includes

- A short description of accelerometric data processing used for comparison with low-resolution Sentinel-2 image correlation.
- A description of the second rupture scenario where rupture would start along the Jordan fault.
- Details about changes of state of stress, slip, and slip-velocity for scenario 1.
- A set of complementary figures:
 - Deformation field and displacement profiles across faults.
 - Correlation of Sentinel-2 images.
 - Slip-distribution along the different faults.
 - Model description and schematic of the FDEM.
 - Definition of the closeness to failure and initial shear traction.
 - Rupture process, displacement field and profiles for scenario 2.
 - Secondary crack network due to dynamic earthquake propagation along with change of stress, slip and slip-velocity in function of time during rupture propagation.
- A table of physical parameters used in modeling.
- Captions for the two movies showing rupture propagation for scenario 1 and 2.

Text S1. Processing of accelerometric data

Datasets from 6 accelerometric stations located in the area affected by the Kaikōura earthquake were processed, from North to South: BWRS, MGCS, SEDS, WDFS, KEKS and KIKS.

Processing follows some of the recipes in Boore and Bommer [2004] for removal of a reference baseline using multi-segment baselines.

Processing steps are:

1. Removal of the linear trend computed on the first third of each acceleration trace (before the P-wave arrival);
2. Rotation of the acceleration records in the ENZ frame, using the information on component orientation available in the StationXML file.
3. Integration to velocity;
4. Manual picking of the starting point of the second linear trend, which appears late on velocity traces. Picking on horizontal and vertical components can be different; an arbitrary uncertainty of +/- 4 seconds is added to the picking.
5. Generation of 10 baseline corrections within the uncertainty range of the manual picking and correction of the velocity components. This produces 10 corrected traces for each component.
6. For each component, integration of the 10 corrected velocity traces to displacement.

7. For each of the 10 displacement traces, static displacement is measured as the average of the last 1000 points (5 sec of trace).
8. For each component, static displacement is defined as the average of the above 10 measures. Measurement variability is given by standard deviation.

Note that no filtering is applied.

Measured static offsets (in meters), with standard deviations								
de: displacement EW, dn displacement NS, du displacement vertical								
Sta	Lon	Lat	de	dn	du	sde	sdn	sdu
BWRS	173.9051	-41.4395	0.0002	0.2429	-0.0266	0.0065	0.0126	0.0018
MGCS	173.9444	-41.5077	-0.5052	0.0935	Nan	0.0456	0.0252	0.0408
SEDS	174.0764	-41.6723	0.7457	1.8544	0.3332	0.0111	0.0322	0.0112
WDFS	174.1384	-41.8274	2.9402	1.3530	1.0011	0.0433	0.1983	0.0340
KEKS	173.9814	-41.9557	5.0039	4.3032	1.7045	0.2572	0.1020	0.0217
KIKS	173.6821	-42.4258	0.1157	-0.2605	0.7642	0.0353	0.1382	0.0038

Boore, D.M. and Bommer, J.J (2005), Processing of strong-motion accelerograms: needs, options and consequences, *Soil. Dyn. Earthq. Eng.*, 25, 93115,
<http://dx.doi.org/10.1016/j.soildyn.2004.10.007>

Text S2. Second scenario: rupture nucleation at the southern end of the Jordan thrust

The model parameters used in this simulation is exactly same with the first scenario discussed in Fig. 3. Figs. S6a-e show the snapshots of the second scenario. In this scenario the rupture propagates northward and activates off-fault cracks. We found a small nucleation of the rupture at the main kink of the Papatea fault as shown in Fig. S6c, which then propagates bilaterally. The rupture propagating southward was in fact trapped as shown in Fig. S6e due to the kink, creating new cracks on the east of Papatea fault. The rupture along the Kekerengu fault accelerated fast enough to transition to supershear speeds as the pre-stress state is partially preferable for a transition to a supershear rupture due to the fault geometry. The nucleation of a daughter crack is clearly seen in Fig. S6c, propagating northward on the Kekerengu fault. Fig. S6f shows the damage pattern and the displacement field at the end of the simulation, where all particle motion ceases. Since the rupture is arrested at the north of the Papatea fault, slip is not observed on the southern part of this fault. Figs. S6g, h show the profiles on the Jordan - Kekerengu fault system and the Papatea fault, respectively. The model is still compatible with the observations on Fig. S6g, whereas it barely fits with observations even with off-fault damage because there is no significant damage to the west of the Papatea fault (Fig. S6h). Furthermore, the localized slip is no longer observed with off-fault damage on profile P2 in Fig. S6h. The deformation in this case simply reflects the large slip on the Jordan – Kekerengu fault system. We therefore conclude that this scenario is less likely than the first scenario.

Text S3. Stress change, slip and slip velocity on the Jordan – Kekerengu fault system and the Papatea fault for the first scenario

We computed the mechanical fields on the two faults separately as shown in Fig. S7. Fig. S7a shows the trace of the Papatea fault and the dynamically activated off-fault cracks plotted in red. Although it forms an intricate crack network around the main kink of the fault, we find a large chain of cracks in the direction towards northwest, which plays a role in the distributed displacement profiles. As the Papatea fault has relatively large kinks and the initial normal and shear tractions on the fault are therefore heterogeneous, the change of normal stress and stress drop along the fault is significant as shown in Figs. S7b-d. The comparison between the model with off-fault damage (in red) and the purely elastic model (in blue) of the change of normal stress indicates that the off-fault medium cannot sustain large stress concentrations as shown at $x/L = 0.72$ in Fig. S7c. We also find a locally negative stress drop around $x/L = 0.72$, where the angle of maximum compressional principal stress is fairly orthogonal and thus the initial shear traction is relatively small. Hence, this part can cause negative stress drop after rupture propagation on such a non-planar fault. Fig. S7e shows the accumulated slip distribution on the Papatea fault. We found a locally enhanced slip in the case with off-fault damage at $x/L = 0.62$ in Fig. S7e, which is directly induced by the off-fault cracks in the vicinity of the fault. Fig. S7f shows the slip velocity in time and space, which shows the detailed rupture process on the Papatea fault. The rupture is initially nucleated around $x/L = 0.3$, propagating bilaterally on the Papatea fault. When the rupture reaches $x/L = 0.7$, it arrests and immediately jumps ahead at $x/L = 0.83$, propagating bilaterally. Eventually the entire Papatea fault is ruptured in this scenario. The slip velocity is remarkably perturbed by the spontaneous off-fault cracking. Since the stress distribution is extremely perturbed by the crack network, negative slip velocity is temporarily induced around $x/L = 0.62$ at $t = 6$ s in Fig. S7f. Figs. S7g-l show the same quantities on the Jordan - Kekerengu fault system. As it has less geometrical complexity compared to the Papatea fault, there is less off-fault damage on the Kekerengu fault as shown in Fig. S7g. The change of normal stress is smoothed by the off-fault damage as shown in Fig. S7i, as is the case for Papatea fault.

Supplementary Figures

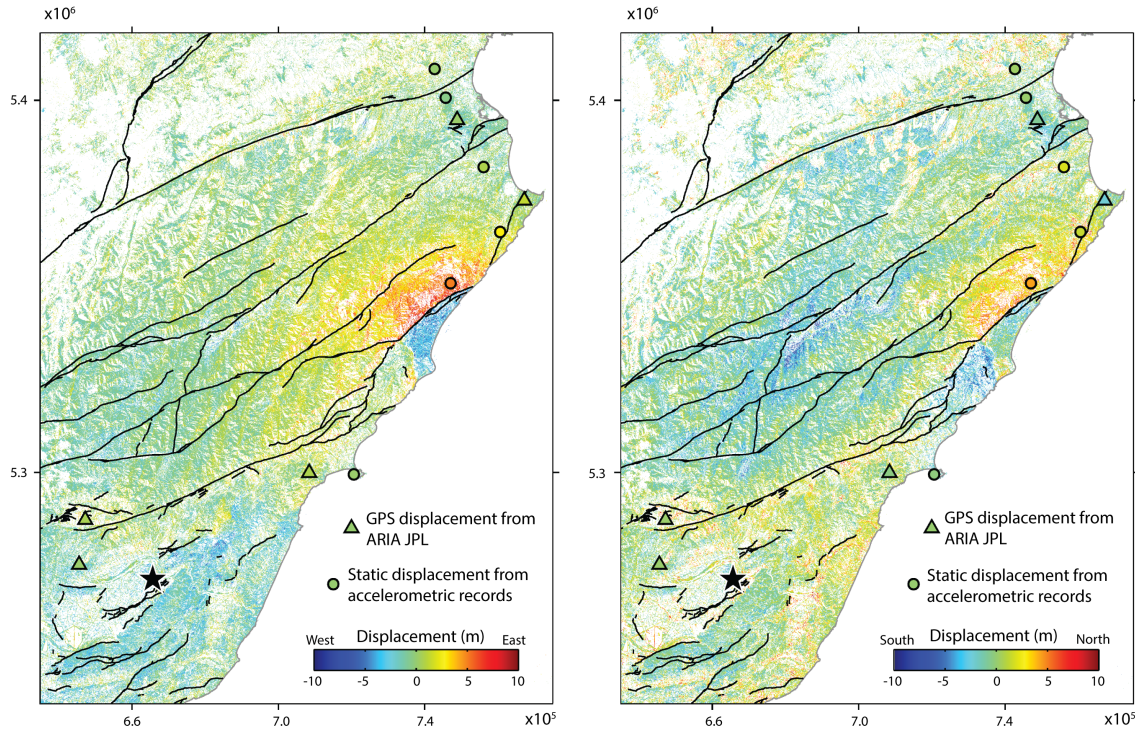


Figure. S1. East-West and North-South components of displacement computed from the correlation of Sentinel-2 images. Coordinates are in UTM. Consistency of the results is checked by comparison with GPS and static motion derived from local strong-motion instruments, for each component. The far-field displacement is set to be zero. The fault network (black lines) is from GNS (<https://data.gns.cri.nz/af/>).

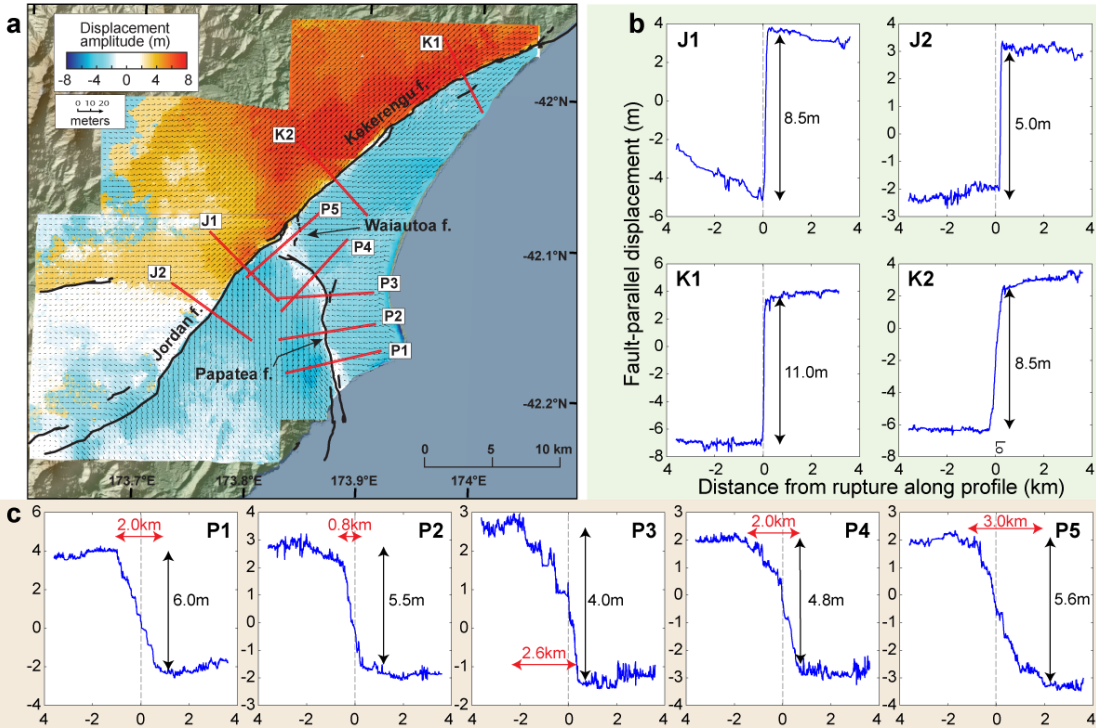


Figure S2. Deformation field and associated displacement profiles. (a) Deformation field around the triple junction with the azimuth of horizontal displacement (arrows). Surface ruptures related to the Kaikoura event are in black [Langridge *et al.*, 2018]. The size of the arrow scales with the amplitude. Arrows converging or diverging from the fault indicate respectively some component of thrust or normal motion. The Papatea block is slightly rotating counter-clock wise. (b) Profiles on the Jordan thrust (J1 and J2) and the Kekerengu faults (K1 and K2). (c) Profiles on the Papatea fault (P1 to P5).

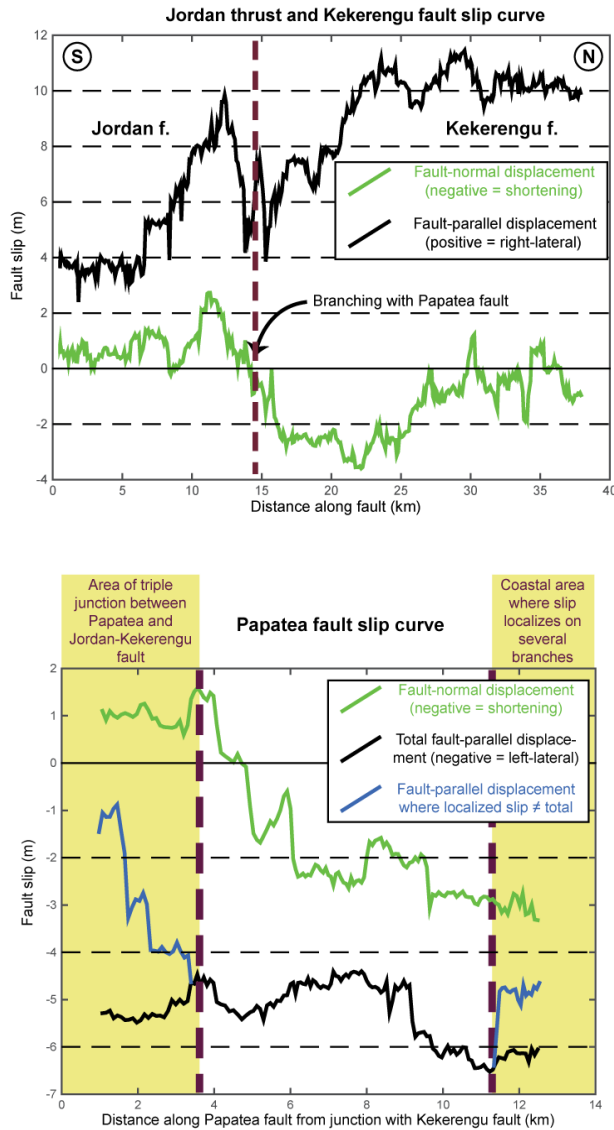


Figure. S3. Slip distribution for the two components of horizontal motion, parallel and perpendicular to the fault, for the Kekerengu – Jordan fault system, and for the Papatea fault. The slip is measured every 90 m, using 8 km-long and 90m wide swaths, with no overlap between successive swaths. The general shape of the slip distribution is consistent with lower resolution slip distribution [Hollingsworth *et al.*, 2017], although details of slip variation can be seen that correspond to variation in fault geometry. The thrust component of the Kekerengu fault and the normal component of the Jordan fault are clearly visible. The thrust component of the Papatea fault is visible almost all along the fault section. The two yellow end boxes indicate locations where the amount of off-fault damage is large.

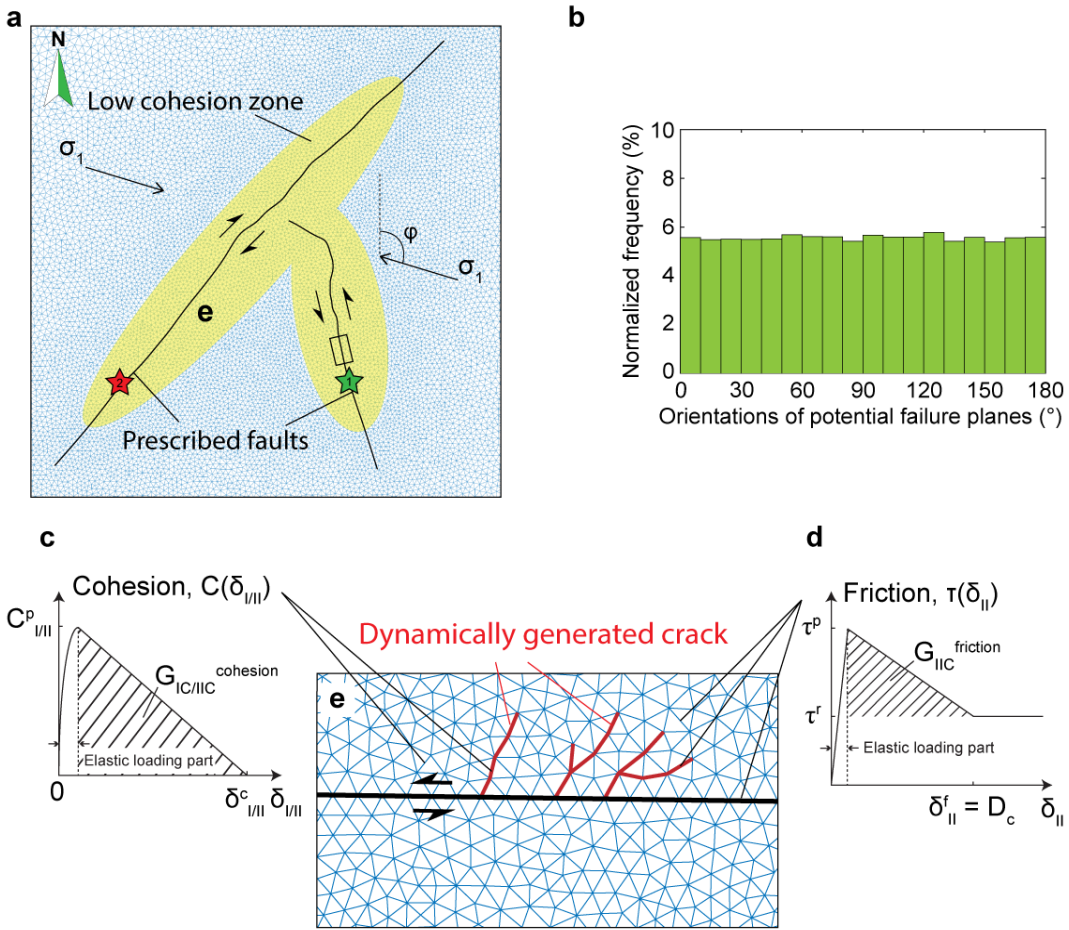


Figure S4. Model description and schematics of FDEM. (a) Schematics of mesh discretization on the prescribed fault system. The Jordan fault, the Kekerengu fault and the Papatea fault are traced as shown in solid black line, according to satellite and field observations. Blue lines show the discrete finite elements. The mesh size is exaggerated for clarity purposes. The overall domain size is 90km x 90km, while the prescribed faults are in 30km x 30km in the middle of the domain to avoid the effects of wave reflections from the domain boundaries. The total number of finite elements is 514,000. σ_1 is the maximum compressional principal stress and φ is the angle of σ_1 to the north. Arrows show the sense of slip. The areas of weakened material are highlighted in yellow. Green and red stars show the position of the rupture nucleation for the first and second scenarios, respectively. Small box shows the zoomed window shown in (e). (b) Histogram of the orientations of the potential failure planes. (c) Linear softening cohesion curve. $\delta_{I/II}$ is the amount of slip in tensile (mode I) and shear (mode II). $C^p_{I/II}$ is the peak cohesive strength in tension and shear. $\delta_{I/II}^c$ is the critical normal/tangential displacement for softening of tensile/shear cohesion. $G_{IC/IIC}^{cohesion}$ is the dissipated energy by breaking cohesion. (d) Linear slip-weakening curve. δ_{II}^f is the characteristic slip distance which is identical with the D_c in conventional slip-weakening law. τ^p and τ^r are the peak and residual strength in friction, derived as $\tau^p = f_s \sigma_n$ and $\tau^r = f_d \sigma_n$, where σ_n is the compressive normal stress on the boundary of elements. $G_{IIC}^{friction}$ is the fracture energy dissipated by the frictional process. (e) Zoomed window around faults shown in (a). Black solid line shows the prescribed fault and blue lines show the finite elements. Red lines show the newly generated cracks on which the cohesion starts to brake due to the stress concentration by the dynamic rupture.

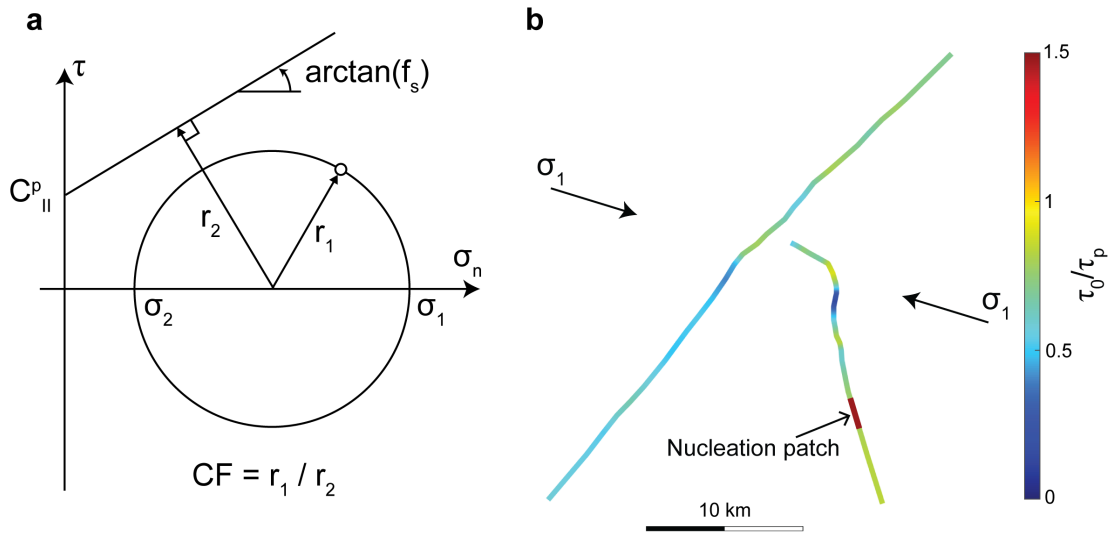


Figure. S5. Definition of closeness to failure (CF) and the initial shear traction. (a) Schematic of closeness to failure, CF, defined as r_1/r_2 . (b) The distribution of initial shear traction normalized by the frictional strength and nucleation patch.

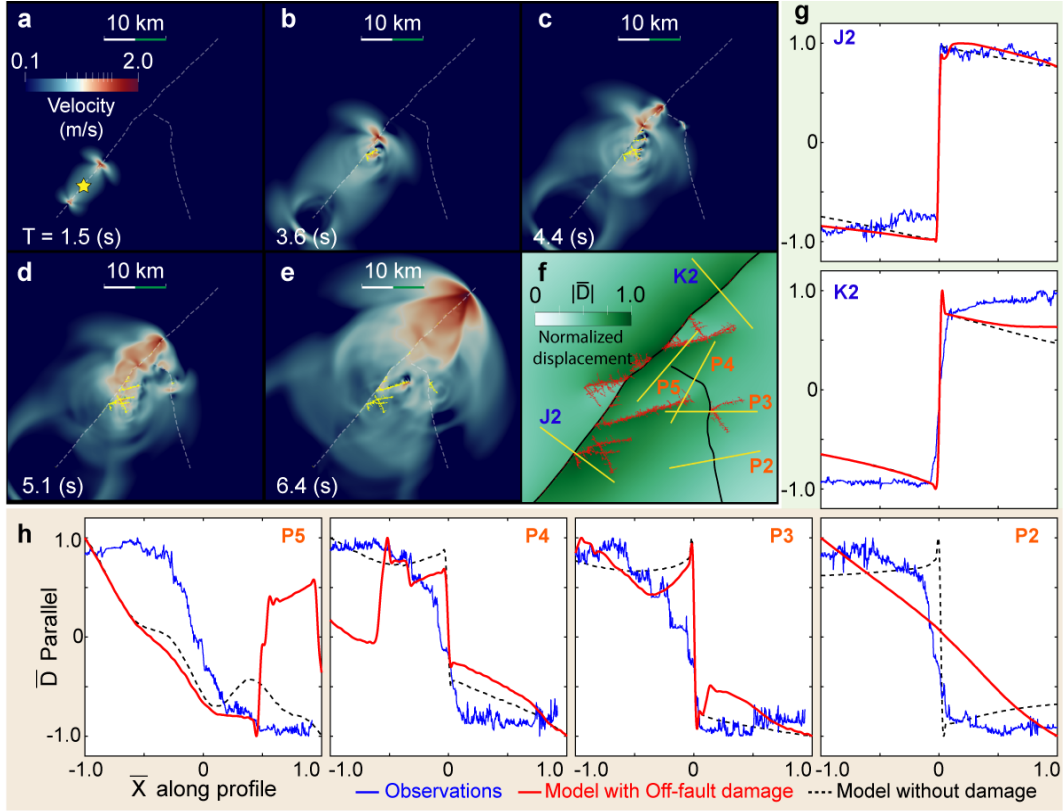


Figure. S6. Rupture process, displacement field and profiles of displacement parallel to the fault for the second scenario. (a-e) Snapshots of the velocity field associated with rupture nucleated from south of Jordan fault (yellow star). Dotted line shows pre-existing faults and yellow lines show the secondary crack network generated by the dynamic earthquake rupture propagation on the main faults. The color contour shows the particle velocity magnitude. (f) The displacement field and the crack network obtained at the end of the earthquake event (at 18s). The yellow lines across the main faults show the position of profiles. (g, h) Measured displacement (blue), modeled displacement including damage (red), and modeled displacement without damage (black dashed) for the different profiles. For comparison, both fault parallel displacements and distance along profiles are scaled by their maximum values.

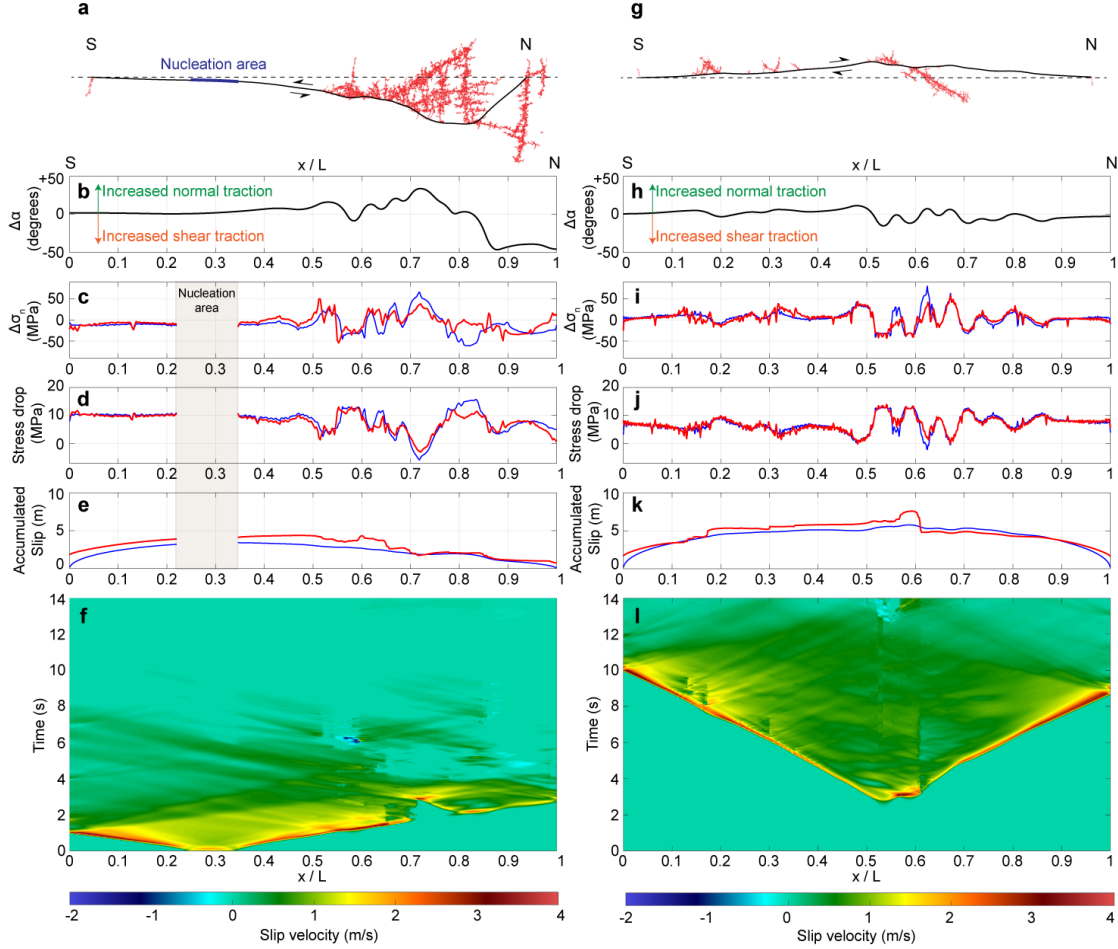


Figure. S7. Off-fault damage pattern, stress change, slip and slip velocity on the Jordan - Kekerengu fault system and the Papatea fault for the first scenario. (a) The trace of secondary crack network generated/activated by dynamic earthquake rupture (in red) on the Papatea fault. The rupture is artificially nucleated at the nucleation segment indicated in blue. Notation S (south) and N (north) show the direction of the fault. The dotted auxiliary line shows a reference to measure the orientation of the maximum compressional principal stress, $\Delta\alpha$, to the fault shown in (b). (b) orientation of the maximum compressional principal stress. $\Delta\alpha$ indirectly indicates the ratio of normal traction to shear traction. Positive values of $\Delta\alpha$ indicate larger normal traction than the reference traction state on the auxiliary line, whereas negative values show smaller ratio of the normal traction to the shear traction. The angle of maximum compressional principal stress to the reference is 53.6° on the Papatea fault and 64.8° on the Jordan - Kekerengu fault system. (c-f) the change of normal stress $\sigma_n^0 - \sigma_n^1$, stress drop $\tau^0 - \tau^1$, accumulated slip and slip velocity, respectively. The red line shows the model with off-fault damage and blue shows the model without off-fault damage. The color contour shows the evolution of the slip velocity on the fault. The horizontal axis shows the position normalized by the length of fault, $x/L = 0$ corresponding to the southern edge of the fault. (g-l) the same quantities on the Jordan - Kekerengu fault system.

Variables	Values	Description
ρ	2700 kg/m ³	Density
E	75 GPa	Young's modulus
μ	30 GPa	Shear modulus
v	0.25	Poisson's ratio
σ_1	45.4 MPa	Maximum compressional principal stress
σ_2	19.1 MPa	Minimum compressional principal stress
φ	107 °	Angle of σ_1 to the north
ds	50 m	Grid size on fault
On prescribed fault		
f_s	0.4	Static friction coefficient
f_d	0.1	Dynamic friction coefficient
$\delta_{II}^f = D_c$	0.17 m	Characteristic slip distance
In off-fault medium		
f_s	0.5	Static friction coefficient
f_d	0.15	Dynamic friction coefficient
$\delta_{II}^f = D_c$	0.017 m	Characteristic slip distance
C_{I}^p	8 MPa / 30 MPa	Peak cohesion for mode I opening crack (Low cohesion zone/the rest of domain)
C_{II}^p	30 MPa / 100 MPa	Peak cohesion for mode II shear crack (Low cohesion zone/the rest of domain)
δ_I^c	2.7 mm	Critical normal displacement for softening of tensile cohesion
δ_{II}^c	7.5 mm	Critical tangential displacement for softening of shear cohesion

Table S1. Parameters used in numerical modeling

Movie S1.

Particle velocity field, slip rate and acceleration records for rupture nucleation on the Papatea fault. The yellow lines correspond to spontaneously activated off-fault cracks.

Movie S2.

Particle velocity field, slip rate and acceleration records for rupture nucleation on the Jordan fault. The yellow lines correspond to spontaneously activated off-fault cracks.